

# **UNRAVELING DEEP GRAY MATTER ATROPHY, IRON AND MYELIN CHANGES IN MULTIPLE SCLEROSIS**

## **ABBREVIATIONS**

DGM = deep gray matter

MS = multiple sclerosis

QSM = quantitative susceptibility mapping

HC = healthy controls

EDSS = Expanded Disability Status Scale

WM = white matter

T2-LL = T2 lesion load

DD = disease duration

## **METHODS**

### *MRI data acquisition*

The acquisition protocol included a 3D T1-weighted Magnetization Prepared Rapid Acquisition Gradient Echo sequence (MPRAGE; TR=2500 ms; TE=2.8 ms; TI=900 ms; Flip Angle=9°; resolution=1x1x1 mm<sup>3</sup>; 176 sagittal slices) used for volumetric analyses, a 3D T2-weighted Fluid Attenuated Inversion Recovery sequence (FLAIR; TR=6000 ms; TE=396 ms; TI=2200 ms; Flip Angle=120°; voxel size=1x1x1 mm<sup>3</sup>; 160 sagittal slices) for the quantification of demyelinating lesion load (T2-LL) volume and two double-echo (TE<sub>1</sub>=7.63 ms; TE<sub>2</sub>=22.14 ms) spoiled gradient echo sequences (Flip Angles of 3° and 20°; TR=28 ms; voxel size=0.7x0.7x1.3 mm<sup>3</sup>; 128 axial slices) for the computation of QSM and R1 map<sup>1-3</sup>.

### *Bulk analysis*

For all patients, hyperintense lesions on FLAIR images were identified and segmented (S.C., with a specific training in brain imaging) using a semiautomatic approach (Jim 7, Xinapse Systems). Lesion masks were then aligned via affine registration to the MPRAGE and used to correct for the possible impact of white matter (WM) lesions on following segmentations via the in-painting procedure implemented in FSL version 5.0.10 (FMRIB's Software Library, [www.fmrib.ox.ac.uk/fsl](http://www.fmrib.ox.ac.uk/fsl))<sup>4</sup>, which replaces lesional voxels with values drawn from the normal appearing WM.

From lesion-filled 3D T1-weighted images, whole brain, total gray matter (GM) and total WM volumes (all normalized for subject head size) were obtained via SIENAX (part of FSL)<sup>5,6</sup>, whereas basal ganglia structures (defined as the caudate, putamen and globus pallidus) and the thalamus were segmented using FIRST (part of FSL)<sup>7</sup>.

For each subject, the R1 map was coregistered to the MPRAGE volume via affine registration, and the corresponding transformation was applied to iron and myelin maps. Segmentation masks were then used to obtain volume (normalized for head size by multiplying

for SIENAX volumetric scaling factor) and mean iron and myelin concentrations for each DGM structure. In addition, as described in by *Hernandez-Torres et al.*<sup>8</sup>, we computed iron mass and myelin mass as measures of total iron and myelin content, respectively, by integrating the concentration maps over each DGM structure (which equates to multiplying the mean value of the concentration map by the number of voxels) and multiplying the result by SIENAX volumetric scaling factor in order to normalize for head size<sup>5</sup>.

#### *Multivariate template construction, voxel-based and thalamic subnuclei ROI analyses*

Initially, susceptibility maps were linearly rescaled such that the voxel values spanned a range typical for T1-weighted imaging<sup>9</sup>. Then, the rescaled QSM and R1 map of all subjects were used to build study-specific multicontrast templates via the `antsMultivariateTemplateConstruction` script implemented in ANTs (Advanced Normalization Tool, version 2.3.1; <http://stnava.github.io/ANTs>)<sup>10</sup>. The template was created by an iterative process. First, all QSMs and R1 maps were coarsely aligned via a rigid registration (using mutual information as similarity metric) to 1mm-isotropic QSM<sup>11</sup> and T1-weighted<sup>12</sup> templates in the Montreal Neurological Institute (MNI) space, respectively, and averaged to produce rough templates, used as the initial targets for a set of four affine registration iterations using cross-correlation. The templates obtained at the end of each iteration were used as new references in the next iteration. To follow, the resulting affine templates were used as the targets for a set of four elastic registration iterations using cross-correlation. Temporary results of the algorithms (at different iteration steps) were visually checked for transformation failures<sup>9</sup>. QSM and R1 maps were used with an equal weighting for driving the registration steps in order to take advantage of their complementary anatomical contrast<sup>9</sup>.

The study-specific QSM template was then coregistered to the reference QSM atlas in the MNI space<sup>11</sup> using the `antsRegistrationSyn` script (part of ANTs)<sup>10</sup>, and the resulting transformations were concatenated and used to bring each subject's iron and myelin maps into the standard space. To take into account the effect of regional atrophy on iron and myelin concentrations at a voxel level, modulated

iron and myelin maps were also computed by scaling with the amount of volume changes due to spatial registration: to this end, spatially normalized unmodulated maps were multiplied by the Jacobian determinant images obtained for the transformations mapping individual native spaces to the standard space. Modulated maps were also multiplied by the SIENAX volumetric scaling factor in order to correct for head size. Both modulated (reflecting local iron/myelin content) and unmodulated (reflecting local iron/myelin concentration) spatially normalized maps were smoothed with a 1-mm FWHM isotropic gaussian kernel before entering the voxel-wise statistical analysis<sup>13</sup>.

In order to investigate possible iron and myelin changes in specific thalamic subregions, ROIs derived from the QSM atlas<sup>11</sup> defining thalamic nuclei (i.e. anterior, lateral, medial, midline nuclear groups and pulvinar) and internal medullary lamina were warped in each subject's native space by applying the inverse of each transformation derived from the previously described coregistration steps. The obtained atlas-based segmentation masks were used to extract volume, iron and myelin values for each thalamic subregion.

**TABLES****Table 1. Portion of MRI contrast attributable to iron or myelin for each DGM structure.**

	<b>Contrast portion</b>	
	<b>Iron</b>	<b>Myelin</b>
<b>Thalamus</b>		
R1	0.42	0.58
QSM	0.88	0.12
<b>Caudate</b>		
R1	0.49	0.51
QSM	0.91	0.09
<b>Putamen</b>		
R1	0.63	0.37
QSM	0.94	0.06
<b>Globus Pallidus</b>		
R1	0.92	0.08
QSM	0.99	0.01

**Table 2. Clusters of significant iron and myelin changes in the DGM of MS patients compared to HC for both the MS > HC and MS < HC contrasts.** Each cluster's volume is presented, along with significance level (FWER-corrected) and the corresponding local maxima's effect sizes, T values and locations. Coordinates refer to mm from the anterior commissure in MNI space, with anatomical labeling according to the AAL atlas<sup>11</sup>.

Contrast	Cluster Volume (ml)	<i>p</i> -value (FWER-corrected)	Cohen's <i>d</i>	T	MNI coordinates (mm)			Anatomical Label
					X	Y	Z	
<b>Unmodulated Iron maps</b>								
MS > HC	4.27	<0.001	1.05	6.26	-17	-12	21	Left Globus pallidus, Caudate, Putamen
	2.16	<0.001	1.09	6.46	17	-7	-3	Right Globus Pallidus, Putamen
	0.73	0.001	0.96	5.67	17	-11	23	Right Caudate
MS < HC	0.70	0.004	1.01	5.98	9	-24	7	Right Thalamus
<b>Modulated Iron maps</b>								
MS > HC	0.34	0.005	0.95	5.62	-13	-3	16	Left Caudate
	0.32	0.006	0.88	5.20	14	-8	19	Right Caudate
MS < HC	1.40	<0.001	1.12	6.65	14	-32	0	Right Thalamus
	0.33	0.003	0.88	5.22	-17	-34	-1	Left Thalamus
<b>Modulated Myelin maps</b>								
MS < HC	1.43	0.004	0.87	5.17	25	-31	0	Right Thalamus
	1.22	0.002	0.93	5.55	-17	-31	2	Left Thalamus

DGM=deep gray matter; HC=healthy controls; FWER=family-wise error rate; MNI=Montreal Neurological Institute.

**Table 3. Results of the ANCOVA analyses for the between-group comparisons regarding thalamic subnuclei.**

Descriptive statistics (means±standard deviations) for thalamic subnuclei MRI features are reported, along with the effect sizes (Cohen's *d*), test statistics (F) and exact probability (*p*-value) values regarding between-group (MS vs HC) comparisons.

	MS	HC	Cohen's <i>d</i>	F	<i>p</i> -value
<b>Normalized Volume (ml)</b>					
Anterior nuclei	0.35±0.05	0.36±0.06	0.29	2.82	0.10
Medial nuclei	1.83±0.36	2.14±0.27	1.15	46.25	<0.001
Midline nuclei	1.00±0.15	1.06±0.14	0.43	6.45	0.01
Lateral Nuclei	3.12±0.57	3.54±0.35	0.96	32.21	<0.001
Internal medullary lamina	3.00±0.49	3.36±0.31	1.05	38.65	<0.001
Pulvinar	2.07±0.55	2.73±0.37	1.34	62.93	<0.001
<b>Iron concentration (mg/kg(DW))</b>					
Anterior nuclei	-1,57±110.36	19.14±76.54	0.19	1.34	0.25
Medial nuclei	38.20±80.57	69.53±74.37	0.46	7.45	0.007
Midline nuclei	-41.02±92.38	20.56±75.71	0.73	18.84	<0.001
Lateral Nuclei	17.57±55.63	9.31±54.41	0.09	0.31	0.58
Internal medullary lamina	-34.46±60.76	-7.95±57.76	0.49	8.49	0.04*
Pulvinar	207.24±109.96	232.38±97.09	0.18	1.19	0.28
<b>Myelin concentration (MVF(DW))</b>					
Anterior nuclei	0.265±0.660	0.262±0.783	0.00	0.00	0.98
Medial nuclei	0.245±0.061	0.226±0.080	0.25	0.01	0.14
Midline nuclei	0.184±0.067	0.187±0.081	0.09	0.00	0.58
Lateral Nuclei	0.338±0.059	0.318±0.079	0.27	0.01	0.11
Internal medullary lamina	0.293±0.060	0.272±0.079	0.27	0.01	0.11
Pulvinar	0.238±0.065	0.224±0.081	0.26	0.01	0.13
<b>Iron content (µg)</b>					
Anterior nuclei	1.07±37.77	6.21±28.47	0.14	0.66	0.42
Medial nuclei	82.80±153.52	154.77±159.92	0.55	10.59	0.001
Midline nuclei	-34.20±87.58	22.79±77.57	0.70	17.38	<0.001
Lateral Nuclei	65.20±171.71	36.37±188.38	0.09	0.35	0.56
Internal medullary lamina	-85.44±162.70	-25.45±191.10	0.39	5.45	0.02*
Pulvinar	462.28±290±89	649.16±315.40	0.59	12.17	0.001
<b>Myelin content (ml)</b>					
Anterior nuclei	0.092±0.027	0.094±0.033	0.14	0.68	0.41
Medial nuclei	0.450±0.154	0.479±0.152	0.27	2.52	0.11
Midline nuclei	0.187±0.091	0.196±0.083	0.18	1.09	0.30
Lateral Nuclei	1.054±0.270	1.120±0.280	0.31	3.36	0.07
Internal medullary lamina	0.865±0.236	0.911±0.264	0.25	2.14	0.15

---

Pulvinar	0.499±0.164	0.599±0.173	0.64	14.41	<0.001
----------	-------------	-------------	------	-------	--------

---

DF=141.

\* Not significant after FDR-correction.

HC=healthy controls; DW=dry weight; MVF=myelin volume fraction; DF=degrees of freedom; FDR=false discovery rate.

**Table 4. Results of the preliminary correlation analyses between clinical data and age- and sex-adjusted standardized residuals of MRI features that emerged as significantly different at the between-group comparisons.**

	Age- and sex-adjusted Z-scores	MS course*	DD (y)	EDSS
DGM structures	<b>Normalized volume</b>			
	Thalamus	-0.528 (<0.001)	-0.261 (0.01)	-0.283 (0.006)
	Caudate	-0.421 (<0.001)	-0.204 (0.05)	-0.224 (0.03)
	Putamen	-0.381 (<0.001)	-0.257 (0.01)	-0.182 (0.09)
	Globus pallidus	-0.421 (<0.001)	-0.225 (0.03)	-0.244 (0.02)
	<b>Iron concentration</b>			
	Thalamus	-0.316 (<0.001)	-0.311 (0.003)	-0.334 (0.001)
	Caudate	0.202 (0.01)	-0.164 (0.12)	-0.154 (0.15)
	Putamen	0.260 (0.002)	-0.110 (0.30)	-0.096 (0.37)
	Globus pallidus	0.318 (<0.001)	0.214 (0.04)	0.003 (0.98)
	<b>Iron content</b>			
	Thalamus	-0.304 (<0.001)	-0.300 (0.004)	-0.324 (0.002)
	Eigenvariates	<b>Unmodulated Iron maps</b>		
Left Basal Ganglia (MS > HC)		0.367 (<0.001)	0.081 (0.44)	-0.041 (0.70)
Right Putamen, Globus Pallidus (MS > HC)		0.412 (<0.001)	0.168 (0.11)	0.004 (0.97)
Right Caudate (MS > HC)		0.386 (<0.001)	-0.036 (0.73)	0.006 (0.96)
Right Thalamus (MS < HC)		-0.352 (<0.001)	-0.267 (0.01)	-0.086 (0.42)
<b>Modulated Iron maps</b>				
Left Caudate (MS > HC)		0.390 (<0.001)	0.014 (0.90)	0.218 (0.04)
Right Caudate (MS > HC)		0.428 (<0.001)	0.003 (0.98)	0.108 (0.31)
Right Thalamus (MS < HC)		-0.400 (<0.001)	-0.233 (0.03)	-0.240 (0.02)
Left Thalamus (MS < HC)		-0.327 (<0.001)	-0.278 (0.008)	-0.292 (0.005)
<b>Modulated Myelin maps</b>				
Right Thalamus (MS < HC)		-0.336 (<0.001)	-0.251 (0.02)	-0.393 (<0.001)
Left Thalamus (MS < HC)		-0.299 (<0.001)	-0.294 (0.005)	-0.338 (0.001)
Thalamic subregions	<b>Normalized volume</b>			
	Medial nuclei	-0.476 (<0.001)	-0.297 (0.004)	-0.088 (0.41)
	Midline nuclei	-0.183 (0.03)	-0.107 (0.31)	0.060 (0.57)
	Lateral Nuclei	-0.434 (<0.001)	-0.250 (0.02)	-0.176 (0.10)
	Internal medullary lamina	-0.472 (<0.001)	-0.261 (0.01)	-0.159 (0.13)
	Pulvinar	-0.564 (<0.001)	-0.262 (0.01)	-0.286 (0.006)
	<b>Iron concentration</b>			
	Medial nuclei	-0.218 (0.008)	-0.282 (0.007)	-0.177 (0.09)
	Midline nuclei	-0.314 (<0.001)	-0.346 (0.001)	-0.192 (0.07)
	Internal medullary lamina	-0.229 (0.005)	-0.227 (0.03)	-0.195 (0.07)
	<b>Iron content</b>			
	Medial nuclei	-0.242 (0.003)	-0.251 (0.02)	-0.132 (0.21)
	Midline nuclei	-0.292 (<0.001)	-0.324 (0.002)	-0.182 (0.09)

Internal medullary lamina	-0.168 (0.04)	-0.201 (0.06)	-0.176 (0.10)
Pulvinar	-0.311 (<0.001)	-0.318 (0.002)	-0.330 (0.001)
<b>Myelin content</b>			
Pulvinar	-0.320 (<0.001)	-0.206 (0.05)	-0.336 (0.001)

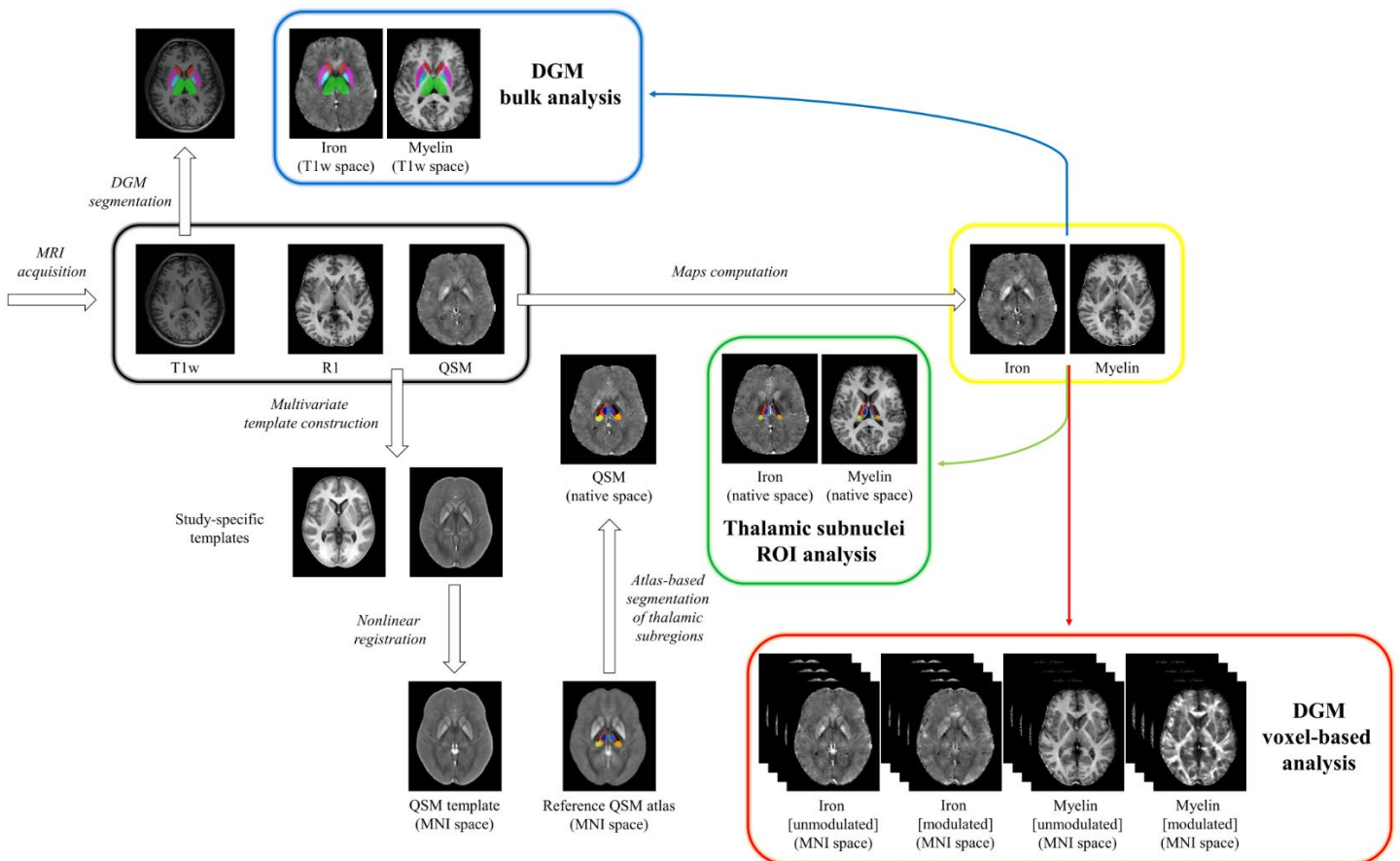
Results are expressed as effect sizes (Pearson's  $r$  or Spearman's  $\rho$ , as appropriate) with  $p$ -values in parentheses.  
 \* Coded with relapsing-remitting as 1 and progressive as 2, such that a negative effect size indicates lower MRI metrics in progressive multiple sclerosis patients.

DD=disease duration; EDSS=Expanded Disability Status Scale.

## FIGURES

**Figure 1. Flow chart summarizing the major steps of the MRI data processing pipeline.** From acquired sequences (*black box*), QSMs and R1 maps were used to compute iron and myelin concentration maps (*yellow box*). DGM structures were automatically segmented on T1-weighted images and the corresponding masks were used for a bulk analysis of iron and myelin mean concentration and global content (*blue box*). Study-specific multicontrast templates were also build based on QSMs and R1 maps, and the resulting spatial transformations were used for an atlas-based segmentation of thalamic subnuclei and investigation of their iron and myelin levels (*green box*), and to bring iron- and myelin-specific maps into the standard space for a voxel-based analysis of iron and myelin changes within DGM structures (*red box*).

DGM=deep gray matter; QSM=quantitative susceptibility mapping; MNI=Montreal Neurological Institute.



## References

1. Palma G, Tedeschi E, Borrelli P, et al. A Novel Multiparametric Approach to 3D Quantitative MRI of the Brain. *PLoS One* 2015;10:e0134963
2. Monti S, Borrelli P, Tedeschi E, et al. RESUME: Turning an SWI acquisition into a fast qMRI protocol. *PLoS One* 2017;12:e0189933
3. Borrelli P, Palma G, Tedeschi E, et al. Improving Signal-to-Noise Ratio in Susceptibility Weighted Imaging: A Novel Multicomponent Non-Local Approach. *PLoS One* 2015;10:e0126835
4. Battaglini M, Jenkinson M, De Stefano N. Evaluating and reducing the impact of white matter lesions on brain volume measurements. *Hum Brain Mapp* 2012;33:2062-2071
5. Smith SM, Zhang Y, Jenkinson M, et al. Accurate, robust, and automated longitudinal and cross-sectional brain change analysis. *Neuroimage* 2002;17:479-489
6. Smith SM, Jenkinson M, Woolrich MW, et al. Advances in functional and structural MR image analysis and implementation as FSL. *NeuroImage* 2004;23 Suppl 1:S208-219
7. Patenaude B, Smith SM, Kennedy DN, et al. A Bayesian model of shape and appearance for subcortical brain segmentation. *Neuroimage* 2011;56:907-922
8. Hernandez-Torres E, Wiggermann V, Machan L, et al. Increased mean R2\* in the deep gray matter of multiple sclerosis patients: Have we been measuring atrophy? *J Magn Reson Imaging* 2019;50:201-208
9. Hanspach J, Dwyer MG, Bergsland NP, et al. Methods for the computation of templates from quantitative magnetic susceptibility maps (QSM): Toward improved atlas- and voxel-based analyses (VBA). *J Magn Reson Imaging* 2017;46:1474-1484
10. Avants BB, Tustison NJ, Song G, et al. A reproducible evaluation of ANTs similarity metric performance in brain image registration. *Neuroimage* 2011;54:2033-2044
11. Zhang Y, Wei H, Cronin MJ, et al. Longitudinal atlas for normative human brain development and aging over the lifespan using quantitative susceptibility mapping. *Neuroimage* 2018;171:176-189

12. Grabner G, Janke AL, Budge MM, et al. Symmetric atlasing and model based segmentation: an application to the hippocampus in older adults. *Medical image computing and computer-assisted intervention : MICCAI International Conference on Medical Image Computing and Computer-Assisted Intervention* 2006;9:58-66
13. Smith SM, Nichols TE. Threshold-free cluster enhancement: addressing problems of smoothing, threshold dependence and localisation in cluster inference. *NeuroImage* 2009;44:83-98